Environmentally-Friendly Cellulose Nanofibre Sheets for Humidity Sensing in Microwave Frequencies

1. Introduction

Humidity sensing has gained increasing interest in terms of becoming an essential assessment tool for a wide range of commercial and industrial applications including environment control, industrial processing and lifestyle improvement [1]. To meet industrial demand, the humidity sensors must satisfy the following requirements: low cost, high sensitivity, high selectivity and wide dynamic range. Given the high dependence of humidity detection systems on sensitive material properties, sensitive materials investigation has become a major field of research for the purpose of improving the commercial competitiveness of humidity sensors [2]. Various materials have been investigated using different technologies for humidity detection including ceramics, organic polymer and organic/inorganic materials [3]. Non-ionic but very polar polyimides and esters are suitable candidates for microwave humidity sensors whose sensing mechanism is based on the variation of dielectric properties as a function of humidity [4]. The effects of moisture on the dielectric constant of some organic polymers films such as Poly(vinyl cinnamate) (PVCi) or Poly(methyl methacrylate) (PMMA) have been investigated through resistive-type or impedance-type sensors in low frequencies [5, 6].

Kapton polyimide and polyvinyl alcohol (PVOH) have been investigated for humidity sensing in RF/microwave frequencies, with the benefits of passive operation as well as integration with RFID technology [7, 8]. The key advantage of Kapton is its compatibility with printing technologies [10, 11] whereas PVOH has shown high sensitivity performances when used alone or when compared to Kapton [12, 13]. A customized polymeric film synthetized from oxidianiline (ODA), *m*-pyromellitic dianhydride (*m*-PMDA), and *N*-methly-2-pyrrolidone (NMP) was also reported [9]. However, due to their fossil nature, all these materials may cause contamination when decomposing in nature. Therefore, it is essential to find more environmentally-friendly remedies to address this problem while maintaining attractive performances for microwave humidity sensing.

Cellulose is the most abundant organic polymer on earth and stands out as a good candidate for environmentally-friendly humidity detection. Cellulose was used as the host-matrix for ceramic particle encapsulation, or blended with organic conducting polymers such as polypyrole and polyaniline (PANI) to form humidity-sensitive composites [15-17]. Cellulose derivatives such as cellulose acetate butyrate (CAB) and Carboxymethyl Cellulose (CMC) were also studied [18, 19]. CAB corresponds to cellulose acetate derivative by grafting of the butyrate group, which makes this material non-biodegradable. For its part, CMC is a matrix that is usually prepared through the reaction of alkali cellulose with monochloroacetate or its sodium salt in and organic medium. CMC was used to improve the humidity response with PANI and Ag-nanocomposite [20, 21]. The PEL Nano P60 paper was studied in printed electronics but required a inorganic coating to achieve absorption of solvents and dispersion agents in the conductive ink [14]. To the best knowledge of the authors, no investigation on pure cellulose and no investigation on fully biodegradable materials for humidity sensing in microwave frequencies has been reported.

This paper presents the cellulose nanofibers (CNF) as new and environmentally-friendly sensitive materials for humidity sensing in microwave frequencies. CNF are nanoscale cellulose with fiber diameter from 5 to 50 nm [22]. Here, CNF were processed through sonocatalysed 2,2,6,6-Tetramethylpiperidinyloxy (TEMPO) oxidation to increase the hydroxyl groups at their surface and improve their affinity to water [23]. No grafting is required. As a final product, CNF are available in the form of foldable sheets of approximately 50 µm thick, making them suitable materials for microwave sensing mechanisms through transmission line technologies, such as the coplanar waveguide (CPW).

This paper investigates the humidity sensing performances of CNF sheets through CPW transmission line technology, well-known for its sensitivity to the surrounding dielectrics. Additional advantages of the CPW structures include low losses compared to microstrip and relatively easy integration with other planar devices. The proposed sensor consists of a CNF sheet taped on the top of the CPW circuit to sense humidity variations in the surrounding environment. The microwave study includes sensitivity analysis through reflected signals with resonant frequency and transmitted signals with phase shift. Furthermore, this paper investigates the influence of the CNF weight by comparing the sensitivity and the dynamic range of sheets with different amounts of CNF.

2. Humidity Sensing Principle

The proposed microwave structure for humidity detection in this paper is a coplanar waveguide (CPW) circuit covered by a CNF sheet on the top as shown in Fig. 1.

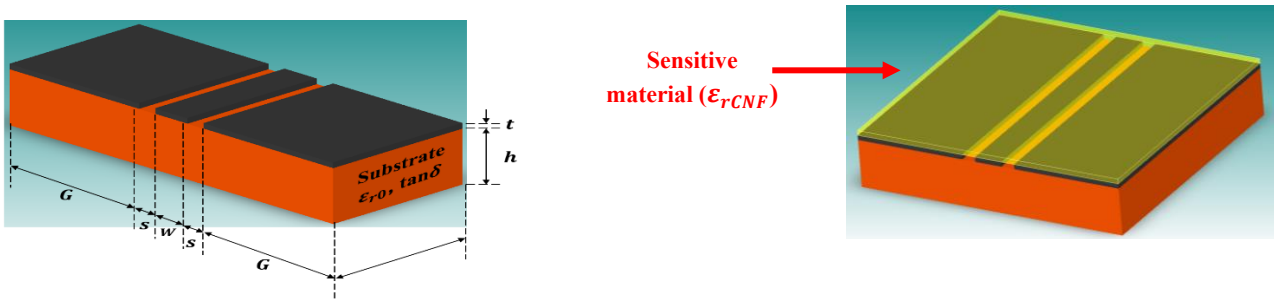

(a) (b)

Fig. 1: CPW structure (a) CPW line with substrate (b) CPW line covered by the sensitive material

The CPW consists of two ground planes surrounding the center signal strip to ensure microwave propagation. The center strip is separated from each ground plane by a narrow gap. The theory of CPW circuits using conformal mapping techniques is presented in [24]. The effective dielectric constant of the circuit presented in 1-b is given in (1). The terms q_0 and q_{CNF} are the partial filling factors of the substrate and the sensitive material respectively. They depend on the substrate thickness (t), the gap dimension (S)

and the trace width (W). The terms ε_{r0} and ε_{rCNF} represent the dielectric properties of the substrate and the CNF sheet respectively.

$$\varepsilon_{eff} = 1 + q_0(\varepsilon_{r0} - 1) + q_{CNF}(\varepsilon_{rCNF} - 1) \quad (1)$$

From (1), the humidity sensing capability can be integrated into the CPW circuit thanks to the hydrophilic or the hydrophobic character of the sensitive material. In this paper, the substrate of the CPW structure is insensitive to humidity so that the effective dielectric constant ε_{eff} closely depends on the dielectric properties of the CNF sheet (ε_{rCNF}) in case of humidity variation. The molecular structure of cellulose is shown in Fig. 2. The polymer backbone contains functional alcohol groups in carbon position 2, 3 and 6. The TEMPO reaction oxidizes the primary alcohol in the carboxyl group as shown in Fig. 3. The abundance of hydroxyl groups and oxygen atoms allows the cellulose to form an extensive network of intra and intermolecular hydrogen bonds, which confers its remarkable chemical stability. The polar groups exert high attraction on water molecules by establishing hydrogen bonds and confer to the cellulose its hydrophilic character.

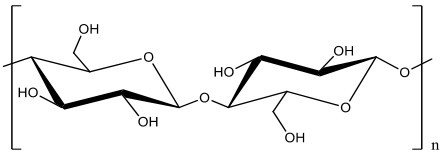

Fig. 2: Molecular structure of cellulose

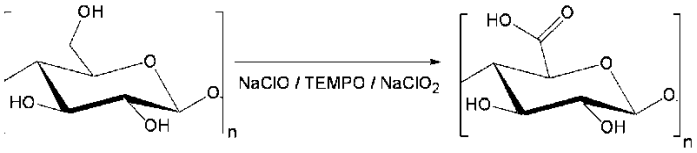

Fig. 3: TEMPO oxidation of cellulose

The humidity absorption by the CNF sheet has two effects. The first effect is the change in its dielectric and conductive properties as a function of humidity. Indeed, humidity absorption modifies the internal electrical state of the CNF and this change is reported to the microwave substrate parameters [4]. The second effect of humidity absorption is the swelling of the CNF films. The presence of beta 1-4 linkage between glucose monomers makes the cellulose insoluble in water so that the sensitive material swells but does not dissolve after humidity absorption. From (1), the change in the dielectric properties and/or the dimensions of the CNF sheet generated by these two effects will be reported on the effective dielectric constant, leading to the change of the characteristic impedance of the CPW circuit as a function of humidity. As a result, reflected and transmitted electromagnetic waves traveling across the circuit will be modified as a function of humidity. Based on this principle, the CPW circuit can be used to monitor humidity variations in the surrounding environment with RF/microwave parameters.

3. Materials and Methods

3.1 Materials

A commercial never-dried bleached Kraft wood pulp was used as the cellulose sample for the production of CNF through TEMPO oxidation and sonication treatments [25]. After a mechanical dispersion, only 20% of cellulose microfibres remain. The carboxyl rate was estimated at 1440 ± 30 mmol/kg and the degree of polymerization was estimated at about 200. The average width and length of nanofibres are about 3.5 ± 1.0 nm and 306 ± 112 nm respectively.

3.2 Preparation of the cellulose nanofibres films and CNF composite films

To prepare the sensitive sheets, cellulose fibres were TEMPO oxidized, to obtain CNF gel at 2.6%. This one was diluted at 0.5% with water. The suspension was then poured into an aluminum dish at different volumes: 40, 60, 80 ml. The Films were dried for two days at ambient air to produce CNF-1, CNF-2 and CNF-3 sheets respectively. Fig. 4 shows the process to obtain CNF sheets.

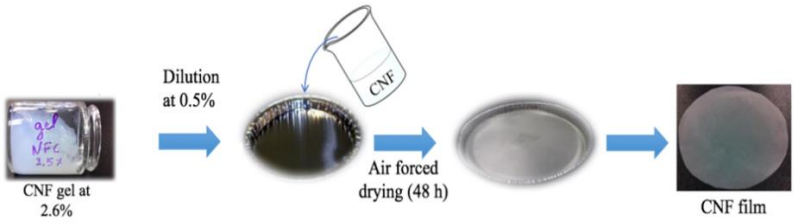

Fig. 4: Schema illustration of CNF films

3.3 Films characterization

3.3.1 Composite structures and films thicknesses

Before all the tests, the samples were preserved at ambient conditions (23°C, 50%RH) for 24 h. The average weight of the samples was determined by measuring of at least ten circular samples with a diameter of 7.8 cm. The weight measurement precision is ± 0.001 g. Average thickness of each sample was determined by image analysis on the cross-sections obtained by a microtome with Scanning Electron Microscopy (SEM) and ImageJ® software. At the same time, surface morphology of the samples was studied using SEM (JEOL-JSM 5500). All samples were covered with gold using a Scientific Instrument PS-2 coating unit for SEM analysis. Infrared spectra were obtained on a Nicolet IS10 FT-IR spectrometer (Thermo Scientific). Each spectrum was acquired in the range of 600–4000 cm^{-1} from 16 scans with the resolution of 4 cm^{-1}. Duplicates of each sample were analyzed at five different points.

3.3.2 Characterization of other physical properties

Thermogravimetric analysis (TGA) allows the thermal stability of materials to be determined by monitoring the weight loss of the sample. Thermal stability of the films was carried out in a Perkin-Elmer (Pyris Diamond) Thermoanalyzer. Samples were heated from 50 to 600 °C under Nitrogen atmosphere at a heating rate of 5 °C/min. The samples were then heated from 600 to 950°C under air at a heating rate of 15 °C/min. In the same way, contact angle measurements were carried out on CNF samples using a Contact angle system OCA20 (DataPhysics). At least 5 drops of water were deposited onto each film.

3.4 Design and fabrication of the microwave sensor

The circuit studied in this paper is a symmetric CPW-based structure derived from [26]. The CPW prototype was fabricated on 4003C substrate from Rogers (ε_r = 3.55, tanδ = 0.0027, thickness of 1.524 mm and 17 µm thickness of copper). This substrate is made of woven glass reinforced hydrocarbon / ceramics. According to the data sheet provided by the manufacturer, its moisture absorption is 0.06% after 48 hours immersion of 60 mil sample at 50 ˚C [27]. This result confirms that the interaction of 4003C with humidity is negligible. The substrate is also insensitive for temperature variation up to 150 ˚C. The characteristic impedance of the CPW line as depicted in Fig. 1-a is set to 50 Ω with W = 4.16 mm and S = 0.3 mm. The ground plane width is G = 14.86 mm and the overall size of the circuit is 5 x 3 cm. As depicted in Fig. 5, the CPW structure dimensions (A,B,C.D and X) have been optimised by electromagnetic simulation with ADS (Advanced Design Systems) tool. Table I gives the values of the CPW structure. The resonant frequency mainly depends on X parameter value [28].

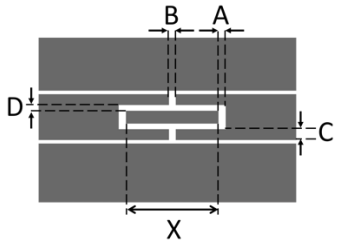

Fig. 5: CPW circuit with structural parameters

Table I: Dimensions values of the CPW structure

Dimensions	A	B	C	D	X
Values (mm)	1.29	0.20	0.70	0.70	23.37

The CPW structure was milled with S103 ProtoMat from LPKF. The S11 and S21 parameters were measured with N9928 vector network analyzer from Agilent. The results are given in Fig. 6. The resonance occurs at 4.642 GHz, with Q-factor of 156. The transmission loss is - 0.658 dB.

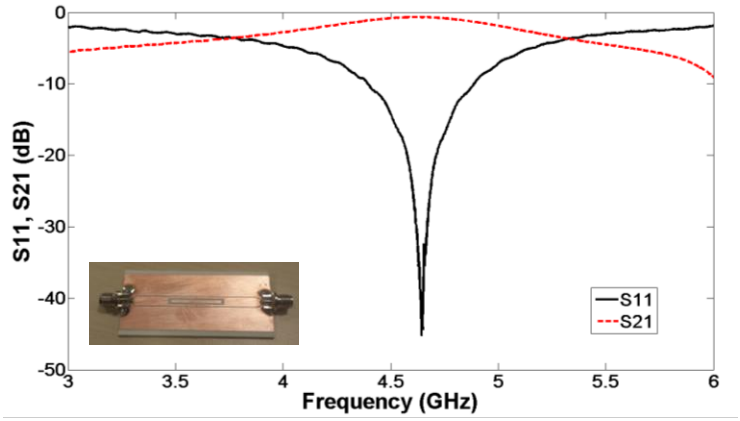

Fig. 6: Reflected signal (S11) and Transmitted signal (S21) measured results of the CPW circuit

To test the humidity sensing performances of CNF sheets, the CPW circuit was fabricated in six prototypes. The CNF sheets were taped on the top of each prototype, using a spray adhesive. To give an example, Fig. 7 shows the fabricated CNF-2 sensor.

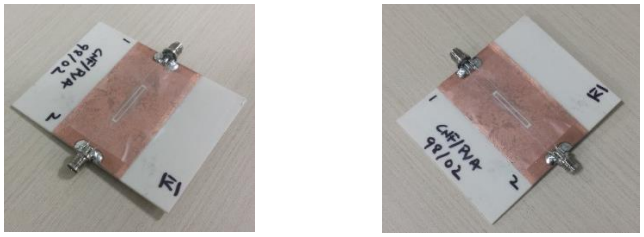

Fig. 7 : CPW circuit with CNF-2 taped as top substrate

3.5 Humidity measurement

The schematic of the humidity detection system is illustrated in Fig. 8-a, and a photograph of this system is presented in Fig 8-b. Humidity is introduced after vaporization at 160 ˚C of the water coming from a pressurised reservoir. The liquid flow controller (LFC) controls the water flow before vaporization, and the mass flow controller (MFC1) helps to measure the humidity mass flow after vaporization. The temperature (T) and the relative humidity (RH) of the mixed gas are measured with the combination of a T/RH probe. This information is used in a feedback loop to control the gas temperature and the relative humidity in the test bench. As mentioned in section 3.4, according to the datasheet, the substrate is insensitive to temperature variations up to 150 ˚C. On the other hand, a temperature of 100 ˚C may cause evaporation of water content in the CNF or in the sample composite. Thus, operating temperature of the sensor must be set under 100 ˚C. In this work, the relative humidity has been measured at 30 ˚C. The HIH4000 from Honeywell is used as reference sensor to give the RH value inside the chamber in real-time. A vacuum pump helps to stabilize pressure inside the chamber. The mass flow controller (MFC2) helps to control the Nitrogen carrier gas flow provided by the cylinder.

The test bench can generate from 0%RH to 100%RH. The tests start in a vacuum with the measured pressure inside the test chamber at 0.03 atm. The Nitrogen gas flow is then raised to 500 sccm to fill the test chamber and the pressure is stabilized at 1 atm. Thereafter, the water flow is set to 1 g/h (LFC) to be vaporized and generate humidity. Nitrogen gas and humidity going inside the mixing box are then apportioned using MFC1 and MFC2. The amount of Nitrogen gas in the mixing box is decreased gradually while the amount of humidity increases accordingly. The mixed gas is then sent to the test chamber where the microwave sensor is located. For each value, a waiting time of 5 minutes was necessary to stabilize the humidity inside the chamber and ensure its absorption by the sensitive substrate. The environmental conditions during the measurement are presented in Fig 8-c.

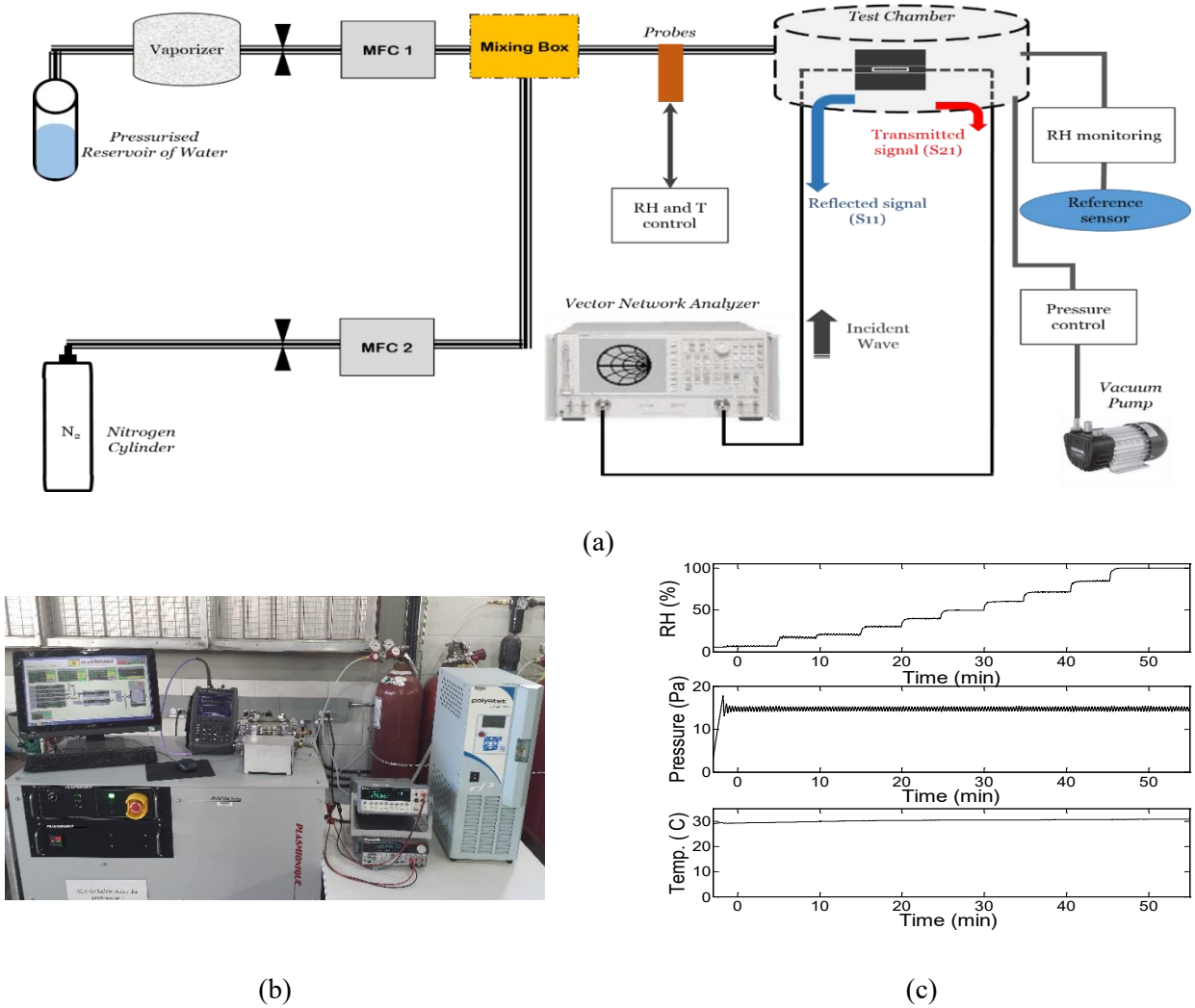

Fig. 8: Environmental conditions during measurement

4. Results and Discussion

4.1 Physical characterization of films

The films appear uniform and slightly opaque. The amount of material used during fabrication will influence the thickness of the films as shown in Table II. The film thickness increases with basis weight. CNF 1 appears thin and flexible while CNF 3 appears more rigid and resistant. The film is thicker making it less flexible.

Table II: Basis weight (g/m^2), thickness (μm) and contact angle (°) of each films.

	Basis weight (g/m^2)	Thickness (μm)	Contact angle (°)
CNF 1	37.7 ± 1.0	22.6 ± 1.9	66.3 ± 4.6
CNF 2	55.5 ± 1.5	30.3 ± 2.1	67.4 ± 5.6
CNF 3	70.9 ± 0.9	36.2 ± 1.6	65.3 ± 5.0

Fig. 9 shows the FTIR spectra of the CNF3 film. The absorption at ~1700 cm^{-1} indicated residual carbonyl (C=O) stretching [29]. CNF absorptions at ~1045 cm^{-1} and 1033 cm^{-1} arise from C–O and O–C–O stretching vibrations. The peaks observed about 3330 cm^{-1} and 1340 cm^{-1} were attributed to O–H stretching, whereas the band at 1380−1310 cm^{-1} is attributed to the anti-symmetric COO− stretching or aliphatic C−H deformation [30]. Finally, the peaks at 2895 cm^{-1} for the C-H and C-C bond, and the peak at 1600 cm^{-1} for the C-O function.

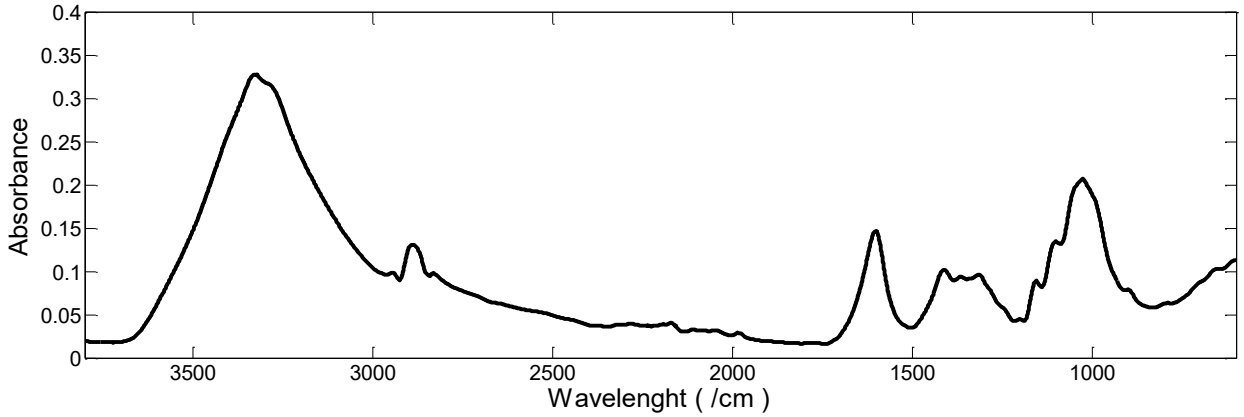

Fig. 9: FT-IR spectra of CNF 3film

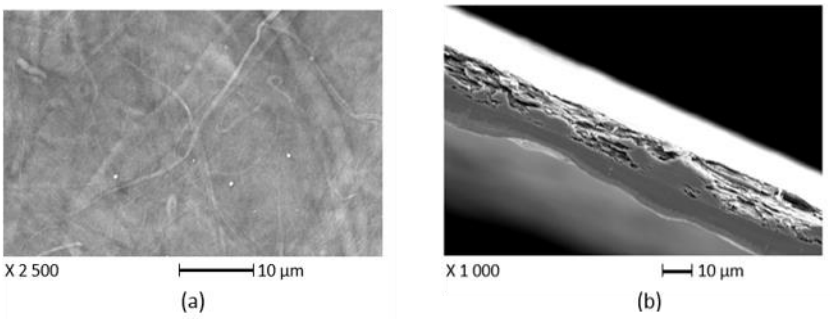

Fig. 10: Surfaces SEM images of (a) CNF film and (b) Cross section of CNF film

Scanning electron microscopy (SEM) images of film showed in Fig. 10-a were analyzed. Images showed a small proportion of cellulose microfibres which is entangled in the nanofibres network. The cellulose nanofibres size was estimated at length ranges from a few µm and width averaging the order of nanometer. The CNF film sheet presents an arrangement of fibres and it is possible to see micro and nanofibres. The underside of films is flat because of the aluminum dish. From the cross section in Fig. 10-b, the network is clearly organized in multiple sheet layers whereas on the upper face, the fibres have regimented in a very dense structure. This situation could be explained by small fibres which sediment at a much slower rate and will be found in increased concentration in the upper section of the film whereas the long fibres are the first to sediment and therefore, found in the lower section of the films.

4.2 Thermogravimetric analysis

The thermogravimetric the curve of CNF3 film is presented in Fig. 11. The film contains few traces of moisture which were eliminated around 110ºC. From Fig. 11, it can be seen that the major weight loss is observed at about 70-80 wt% in the range of 180-450ºC. As shown in the thermogravimetric curve, the cellulose begins to deteriorate at 185ºC. CNF3 appears to decompose between 190 ºC and 300 ºC. The corresponding weight loss was attributed to the destruction of the crystalline region. After 680ºC the graph shows complete decomposition of the sample.

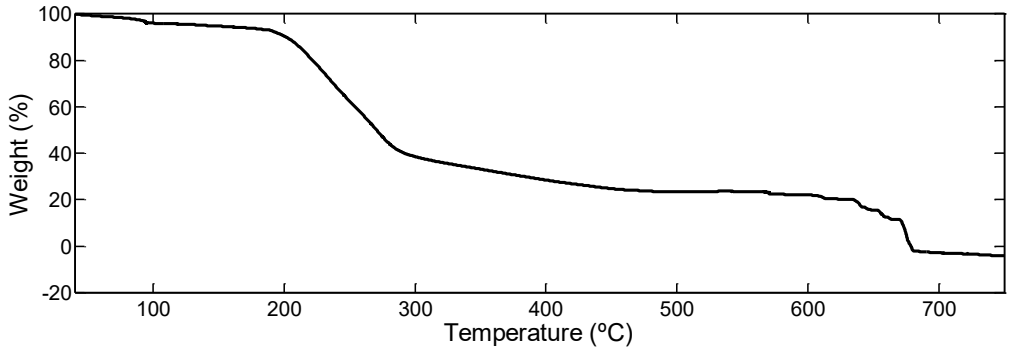

Fig. 11: Thermogravimetric analysis of CNF3

4.3 Contact angle

To confirm the affinity of our system as a humidity sensor, contact angle measurements were made on the different films. The results are shown in Table II. The contact angle is around 66° for CNF films. It is well known that cellulose is a hydrophilic material and has high water affinity. Indeed, for a pure cellulose film, the contact angle is relatively small. However, the contact angle will depend on the materials structure. Due to their small sizes, the use of cellulose nanofibres will create a much denser network than cellulose fibres. The surface becomes smoother and less porous. The contact angle is then increased. The high water affinity is reduced by the dense network. However, the cellulose wettability is slightly affected since all of the drop is absorbed by the film after one minute.

4.4 Humidity response

This section presents the measured humidity responses. Measurements have been realized three times for each sample to ensure the repeatability of the results. Only the mean values are presented. The first parameter studied to investigate sensing performances of the proposed microwave sensors is the resonant frequency. The resonant frequency helps to study the humidity sensing mechanism with reflected waves travelling along the CPW circuit. The focus of this study is to integrate CNF in 1-port microwave devices for humidity detection. As the humidity increases in the surrounding environment, the resonant frequency of each sensor shifts accordingly. The measured shifting depends on the humidity sorption properties of the CNF sensitive sheets. The results are presented in Fig. 12. The second parameter studied to investigate the sensing performances of the proposed microwave sensors is the S21 phase. The S21 phase helps to study the humidity sensing mechanism with transmitted waves travelling along the CPW circuit. Here, the sensor responds to humidity variation by S21 phase angular shift. This study is original and interesting in integrating CNF with 2-port microwave devices such as phase shifters and delay lines for humidity detection. Fig. 13 shows the S21 phase shifts at 4.5 GHz in various humidity conditions for CNF sensitive sheets. From 0%RH to 100%RH, the overall resonant frequency shifts and S21 phase shifts are presented in Table III.

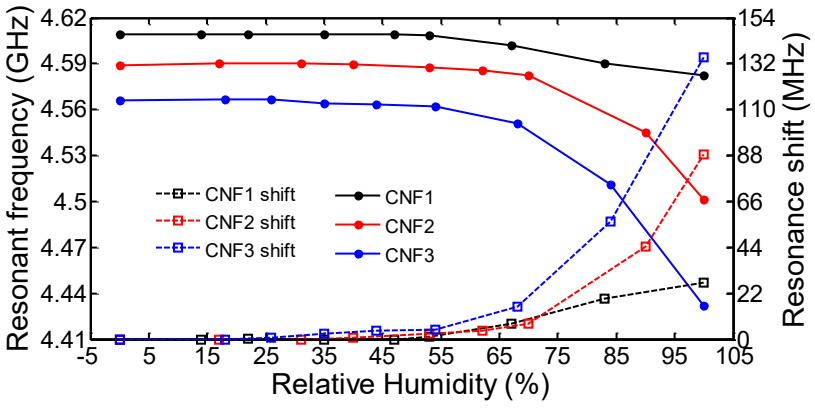

Fig. 12: Resonant frequency of CNF films as a function of RH

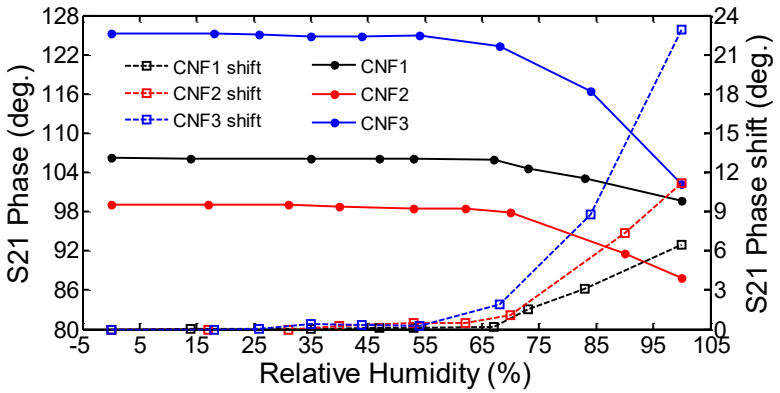

Fig. 13: S21 parameter of CNF films as a function of RH

Table III: Mesures performances of CNF composite films

Covering films	CNF1	CNF2	CNF3
Total frequency shift (MHz)	27.2	88.7	135.0
Total S21 Phase shift (°)	6.49	11.20	22.95
Maximum losses (dB)	-1.40	-2.44	-3.09
Figure of merit (°/dB)	4.63	4.59	7.43

Table IV summarizes all the results obtained in this article. The humidity sensitivity and the dynamic range are presented. For the humidity dynamic range from RH_1 to RH_2 value, corresponding to the target parameter shift (δ) from δ_1 to δ_2, the sensitivity (S_{RH}^{δ}) here is given in (2). The target parameters include resonant frequency and S21 phase.

$$S_{RH}^{\delta} = \left|\frac{\Delta\delta}{\Delta(RH)}\right| = \left|\frac{\delta_2 - \delta_1}{RH_2 - RH_1}\right| \qquad (2)$$

Table IV: Measured sensitivities for CNF and CNF sheets

Sheets	Resonant frequency (MHz/%RH)	RH range (%RH)	S21 Phase (°/%RH)	RH range (%RH)
CNF1	-	20 – 55	0.010	0 – 70
	0.645	55 – 100	0.192	70 – 100
CNF2	0.138	20 – 55	0.013	0 – 70
	2.164	55 – 100	0.337	70 – 100
CNF3	0.167	20 – 55	0.025	0 – 70
	2.826	55 – 100	0.702	70 – 100

First from measurement results, the sensor sensitivity increases as the amount of CNF increases. This can be explained precisely by the CNF weight. Indeed, the more concentrate the CNF film is, more water it can absorb and the better will be the sensitivity. The best results are obtained with the CNF3 sheet whose sensitivity is 0.167 MHz/%RH from 20%RH-55%RH, and 2.826 MHz/%RH from 55%RH-100 %RH. The qualitative similarity of S21 phase and resonant frequency responses to RH confirms that they all originate from the same mechanism that is the CPW effective permittivity sensitivity to RH. The best results for the S21 phase shift are obtained with the CNF3 sheet that is 0.702 °/%RH in the 70%RH-100%RH humidity range. Other analyses were carried out to evaluate the performance degradation of the CPW structure acting as humidity sensor. Fig. 14 show the S21 parameter variation at the resonance to study the evolution of transmission losses. The S21 variations are presented in Table III.

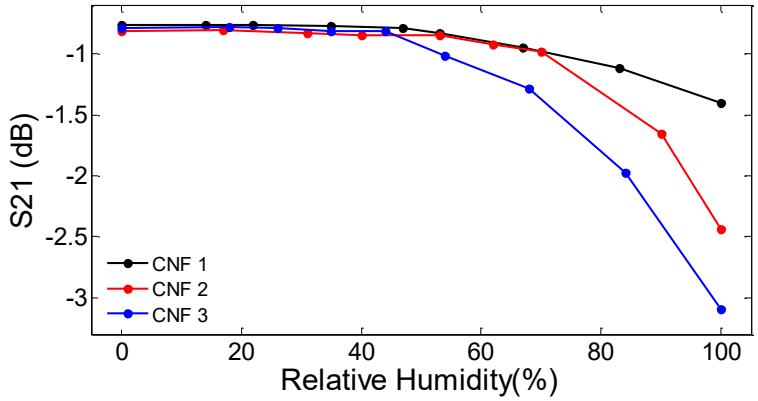

Fig. 14: S21 parameter of CNF films as a function of RH

For all the circuits, the transmission losses increase as the humidity increases. Since the permittivity increases with the humidity absorption increases, the electromagnetic field encounters a higher resistance during the propagation. As a result, the transmission losses increase. This also induces the degradation of the Q-factor of the CPW structure since the dielectric losses increase accordingly. However, the maximum loss measured is -3.09 dB for CNF3 which remains attractive for a CPW line. When operating as phase shifter, the figures of merit as defined in [31] are also presented in Table III. The CNF3 sheet has the best performances that is 7.43 °/dB. Compared to all the previous results, CNF3 is the best sensitive sheet studied in this paper.

4.5 Dynamic range and hysteresis analysis

The humidity response to humidity is not very good in low humidity levels. Even if the reason is not very clear, some hypotheses can be made to explain this result. That is to say, water molecules are attracted by the hydroxyl groups within the CNF molecular structure. Below 30 %RH – 35 %RH, the humidity absorption remains superficial and only a small part of water molecules diffuse through the substrate. As a result, the permittivity variation is not important enough to change microwave parameters of the CPW

circuit. However, as the humidity increases, more water is absorbed and diffuses through the substrate, leading to a most marked change in the permittivity and an increased swelling of the substrate. Moreover, the electromagnetic field propagation of the CPW structure is affected by environment. All these mechanisms lead to the increase of sensitivity of the sensor as the humidity increases. Reversely, when humidity reduces, water molecules are released and the circuit retrieves its initial states. There is no patent hysteresis effect. Fig. 15 shows the humidity response of CNF3 during absorption and desorption of humidity.

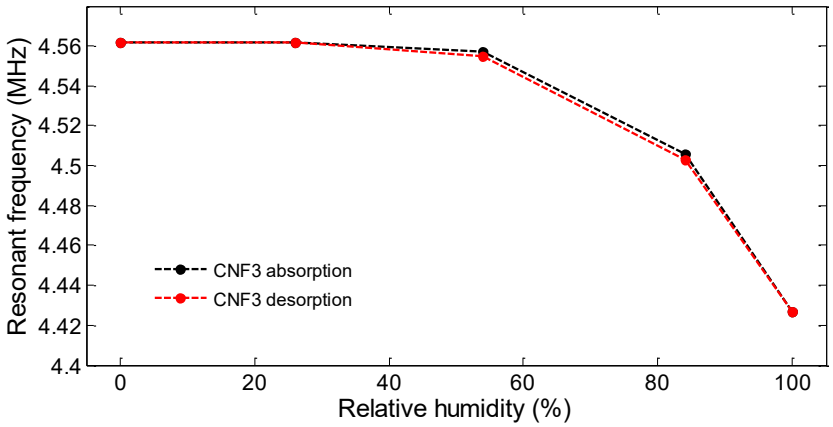

Fig. 15: CNF3 absorption and desorption

4.6 Comparison

Previous microwave humidity sensors based on sensitive substrates were reported. Some of the proposed structures were tested in air, and some structures were tested in other environments including Nitrogen-containing environment [32] and saturated salt solutions [10]. For the results to be valid, the condition is that the sensor should not react to the environment composition but only to humidity variation. In this paper, Nitrogen gas is used as carrier. CNF is insentitive to Nitrogen and only react to the humidity variation. Thus, the results of this work can be compared to that of previous works. Table V compares the performances of CNF sheets introduced in this work to previous research investigating sensitive substrates in the RF/microwave frequencies for humidity detection. Only the best performances for each reference have been reported. Various sensing mechanisms have been investigated with PEL paper, Kapton and PVOH including (1) resonant frequency variation of LC-type resonator and stepped-impedance resonator [7, 8, 12-14], and (2) radiated power variation of a RF integrated circuit connected with parallel plates sandwiching the sensitive substrate [11]. The highest sensitivity reported for PEL paper, Kapton and PVOH is respectively 0.53 MHz/%RH, 1.68 MHz/%RH and 6.75 MHz/%RH. PVOH exhibits the best sensitivity but is not biodegradable. The best result measured in this paper is 2.82 MHz/%RH, with the CNF3 sample. CNF3 appears more sensitive than PEL paper and Kapton, while being compatible to printing technologies as well. Indeed, the surface energy of CNF3 is 50 dyne/cm^2 and the material may encounter thermal sintering up to 100 ˚C. The results presented in this paper cover a large range of RH

values compared to most of the previous research. Beyond the previous works, this paper studied the phase variation due to humidity-sensitive dielectrics in transmission line technology. The best S21 phase sensitivity was measured with CNF3 at 0.7 °/%RH.

Table V: Comparison of the performances of CNF and CNF sheets to previous research investigating humidity-sensitive substrates in the RF/microwave frequencies

Substrates	Resonant frequency (MHz/%RH)	RH range (%RH)	S21 Phase (°/%RH)	RH range (%RH)	Microwave structures	Ref.
Kapton	0.20	11 – 97			Double-sided parallel-plates	[11]
	0.64	80 – 90			Stepped-impedance resonator	[7]
	1.68	35 – 85			ELC resonator	[13]
	1.36	35 – 85			ELC resonator	[8]
PVOH	6.75	50 – 90			ELC resonator	[13]
	5.35	50 – 100			PVOH coated IDC	[12]
PEL paper	0.53	20 – 90			LC resonator	[14]
CNF3	0.17	20 – 55	0.025	0 – 70	**CPW-based circuit**	**This work**
	2.82	**55 – 100**	**0.70**	**70 – 100**		

5. Conclusion

This paper investigated environmentally-friendly cellulose nanofibres (CNF) as new and sensitive material for humidity sensing in RF/microwave frequencies. CNF sheets were fabricated, oxidized by sonocatalyzed TEMPO process and physically characterized. Humidity sensing investigation was performed with CNF sheets stacked on the top of CPW-based circuits. This investigation includes sensitivity and dynamic range analysis through reflected waves along the CPW circuit with resonant frequency shift, and transmitted waves with phase shift. Sheets with various amounts of CNF have been used to study the influence of CNF weight on humidity sensing performances. Regarding the resonant frequency shift, the best sensitivity was measured with the weightier CNF film (71 g/m^2), that is 2.82 MHz/%RH from 55%RH to 100%RH. As a phase shifter, the same film sensitivity is 0.7 °/%RH from 70%RH to 100%RH, with a figure of merit of 7.43 °/dB.

This work is a proof-of-concept to validate the humidity sensitivity with TEMPO oxidized CNF. Further investigation is now considered. The next step will be the investigation of the printing potential of CNF. This is very realistic since the surface energy of the CNF sheets was measured at 50 dyne/cm^2, then allowing adherence of inkjet and screen printing inks. Such study will lead to lower cost, higher sensitive and more environmentally-friendly humidity sensors.

6. References

[1] T. A. Blank, L. P. Eksperiandova, and K. N. Belikov, "Recent trends of ceramic humidity sensors development: A review," *Sensors and Actuators B: Chemical,* vol. 228, pp. 416-442, 6/2/ 2016.

[2] H. Farahani, R. Wagiran, and M. N. Hamidon, "Humidity Sensors Principle, Mechanism, and Fabrication Technologies: A Comprehensive Review," *Sensors,* vol. 14, pp. 7881-7939, 2014.

[3] C.-Y. Lee and G.-B. Lee, "Humidity sensors: a review," *Sensor Letters,* vol. 3, pp. 1-15, 2005.

[4] Z. Chen and C. Lu, "Humidity sensors: a review of materials and mechanisms," *Sensor letters,* vol. 3, pp. 274-295, 2005.

[5] M. Matsuguchi, S. Umeda, Y. Sadaoka, and Y. Sakai, "Characterization of polymers for a capacitive-type humidity sensor based on water sorption behavior," *Sensors and Actuators B: Chemical,* vol. 49, pp. 179-185, 7/1/ 1998.

[6] Y. Sakai, Y. Sadaoka, and M. Matsuguchi, "Humidity sensors based on polymer thin films," *Sensors and Actuators B: Chemical,* vol. 35, pp. 85-90, 1996.

[7] E. M. Amin and N. C. Karmakar, "Development of a low cost printable humidity sensor for chipless RFID technology," in *RFID-Technologies and Applications (RFID-TA), 2012 IEEE International Conference on*, 2012, pp. 165-170.

[8] E. M. Amin, M. S. Bhuiyan, N. C. Karmakar, and B. Winther-Jensen, "Development of a Low Cost Printable Chipless RFID Humidity Sensor," *Sensors Journal, IEEE,* vol. 14, pp. 140-149, 2014.

[9] Y.-H. Kim, K. Jang, Y. J. Yoon, and Y.-J. Kim, "A novel relative humidity sensor based on microwave resonators and a customized polymeric film," *Sensors and Actuators B: Chemical,* vol. 117, pp. 315-322, 10/12/ 2006.

[10] A. Rivadeneyra, J. Fernández-Salmerón, M. Agudo, J. A. López-Villanueva, L. F. Capitan-Vallvey, and A. J. Palma, "Design and characterization of a low thermal drift capacitive humidity sensor by inkjet-printing," *Sensors and Actuators B: Chemical,* vol. 195, pp. 123-131, 2014.

[11] J. Virtanen, L. Ukkonen, T. Bjorninen, A. Z. Elsherbeni, Syda, x*, et al.*, "Inkjet-Printed Humidity Sensor for Passive UHF RFID Systems," *Instrumentation and Measurement, IEEE Transactions on,* vol. 60, pp. 2768-2777, 2011.

[12] D. Lu, Y. Zheng, M. Schussler, A. Penirschke, and R. Jakoby, "Highly sensitive chipless wireless relative humidity sensor based on polyvinyl-alcohol film," in *Antennas and Propagation Society International Symposium (APSURSI), 2014 IEEE*, 2014, pp. 1612-1613.

[13] E. M. Amin, N. C. Karmakar, and B. Winther-Jensen, "Polyvinyl-alcohol (pva)-based rf humidity sensor in microwave frequency," *Progress In Electromagnetics Research B,* vol. 54, pp. 149-166, 2013.

[14] Y. Feng, L. Xie, Q. Chen, and L. R. Zheng, "Low-Cost Printed Chipless RFID Humidity Sensor Tag for Intelligent Packaging," *IEEE Sensors Journal,* vol. 15, pp. 3201-3208, 2015.

[15] S. Ummartyotin and H. Manuspiya, "A critical review on cellulose: From fundamental to an approach on sensor technology," *Renewable and Sustainable Energy Reviews,* vol. 41, pp. 402-412, 1// 2015.

[16] S. K. Mahadeva, S. Yun, and J. Kim, "Flexible humidity and temperature sensor based on cellulose–polypyrrole nanocomposite," *Sensors and Actuators A: Physical,* vol. 165, pp. 194-199, 2// 2011.

[17] S. K. Shukla, "Synthesis and characterization of polypyrrole grafted cellulose for humidity sensing," *International Journal of Biological Macromolecules,* vol. 62, pp. 531-536, 11// 2013.

[18] F. Molina-Lopez, D. Briand, and N. F. de Rooij, "All additive inkjet printed humidity sensors on plastic substrate," *Sensors and Actuators B: Chemical,* vol. 166–167, pp. 212-222, 5/20/ 2012.

[19] S. Kotresh, Y. T. Ravikiran, H. G. Raj Prakash, C. V. V. Ramana, S. C. Vijayakumari, and S. Thomas, "Humidity sensing performance of spin coated polyaniline–carboxymethyl cellulose composite at room temperature," *Cellulose,* vol. 23, pp. 3177-3186, 2016.

[20] S. Kotresh, Y. Ravikiran, H. R. Prakash, C. V. Ramana, S. Vijayakumari, and S. Thomas, "Humidity sensing performance of spin coated polyaniline–carboxymethyl cellulose composite at room temperature," *Cellulose,* vol. 23, pp. 3177-3186, 2016.

[21] W. Marzouk, N. Sakly, S. Roudesli, H. Ben Ouada, and H. Majdoub, "Ag-nanocomposite based on carboxymethylcellulose for humidity detection: Green synthesis and sensing performances," *Journal of Applied Polymer Science,* vol. 133, pp. n/a-n/a, 2016.

[22] M. Paquin, É. Loranger, V. Hannaux, B. Chabot, and C. Daneault, "The use of Weissler method for scale-up a Kraft pulp oxidation by TEMPO-mediated system from a batch mode to a continuous flow-through sonoreactor," *Ultrasonics sonochemistry,* vol. 20, pp. 103-108, 2013.

[23] B. Puangsin, Q. Yang, T. Saito, and A. Isogai, "Comparative characterization of TEMPO-oxidized cellulose nanofibril films prepared from non-wood resources," *International journal of biological macromolecules,* vol. 59, pp. 208-213, 2013.

[24] R. N. Simons, *Coplanar waveguide circuits, components, and systems* vol. 165: John Wiley & Sons, 2004.

[25] A. Rattaz, S. P. Mishra, B. Chabot, and C. Daneault, "Cellulose nanofibres by sonocatalysed-TEMPO-oxidation," *Cellulose,* vol. 18, pp. 585-593, 2011.

[26] K. Hettak, N. Dib, A. F. Sheta, and S. Toutain, "A class of novel uniplanar series resonators and their implementation in original applications," *Microwave Theory and Techniques, IEEE Transactions on,* vol. 46, pp. 1270-1276, 1998.

[27] R. Corporation. *https://www.rogerscorp.com/*.

[28] K. C. Gupta, *Microstrip lines and slotlines*, 2nd ed. ed. Boston: Artech House, 1996.

[29] S. Wu, F. Li, H. Wang, L. Fu, B. Zhang, and G. Li, "Effects of poly (vinyl alcohol)(PVA) content on preparation of novel thiol-functionalized mesoporous PVA/SiO 2 composite nanofiber membranes and their application for adsorption of heavy metal ions from aqueous solution," *Polymer,* vol. 51, pp. 6203-6211, 2010.

[30] J. Araki, M. Wada, and S. Kuga, "Steric stabilization of a cellulose microcrystal suspension by poly (ethylene glycol) grafting," *Langmuir,* vol. 17, pp. 21-27, 2001.

[31] O. G. Vendik, I. B. Vendik, and M. A. Nikol'ski, "Comparison of MMIC phase shifters using figure of merit as the main characteristic," in *Microwaves, Radar and Wireless Communications, 2004. MIKON-2004. 15th International Conference on*, 2004, pp. 333-335 Vol.1.